

Safe and Economical UAV Trajectory Planning in Low-Altitude Airspace: A Hybrid DRL-LLM Approach with Compliance Awareness

Yanwei Gong, Xiaolin Chang

Abstract—The rapid growth of the low-altitude economy has driven the widespread adoption of unmanned aerial vehicles (UAVs). This growing deployment presents new challenges for UAV trajectory planning in complex urban environments. However, existing studies often overlook key factors, such as urban airspace constraints and economic efficiency, which are essential in low-altitude economy contexts. Deep reinforcement learning (DRL) is regarded as a promising solution to these issues, while its practical adoption remains limited by low learning efficiency. To overcome this limitation, we propose a novel UAV trajectory planning framework that combines DRL with large language model (LLM) reasoning to enable safe, compliant, and economically viable path planning. Experimental results demonstrate that our method significantly outperforms existing baselines across multiple metrics, including data collection rate, collision avoidance, successful landing, regulatory compliance, and energy efficiency. These results validate the effectiveness of our approach in addressing UAV trajectory planning key challenges under constraints of the low-altitude economy networking.

Index Terms—Data Collection, Large Language Model, Reinforcement Learning, Low-Altitude Economy, Trajectory Planning

I. INTRODUCTION

With the rapid advancement of the low-altitude economy, low-altitude airspace has emerged as a critical strategic resource for driving urban intelligence, industrial upgrading, and digital economic transformation [1]. This evolving domain integrates diverse sectors such as general aviation and urban air mobility, wherein unmanned aerial vehicles (UAVs) play an increasingly vital role in applications including logistics, agricultural monitoring, infrastructure inspection, and environmental protection [2]. Efficient utilization of this low-altitude airspace presents unprecedented opportunities for industry growth and technological innovation.

In this context, UAV-based data acquisition represents a fundamental technology enabling high-precision, multi-modal environmental sensing [3]. The UAV data acquisition process typically involves task assignment, flight trajectory planning, sensor data collection, and data transmission and processing. Effective trajectory planning is crucial for maximizing area coverage and data quality, thereby supporting downstream applications with accurate and timely information [4].

Despite its potential, the trajectory planning for UAV data acquisition in low-altitude airspace faces the following considerable challenges:

- **Robust Obstacle Avoidance in Urban Airspaces.** Operating in low-altitude urban environments exposes data collection UAVs (DCUs) to both static obstacles (e.g., buildings) and dynamic obstacles (e.g., other UAVs). These obstacles are often partially observable and highly uncertain. Moreover, DCUs must also avoid restricted no-fly zones (NFZs) over sensitive areas. Ensuring robust obstacle avoidance under such conditions remains a core challenge. Traditional optimization methods typically lack the adaptability to handle such stochastic environments, and standard deep reinforcement learning (DRL) struggles to accumulate sufficient successful trajectories, leading to low learning efficiency.
 - **Intelligent Planning for the Balance of Efficiency, Economy, and Compliance.** In the low-altitude economy, DCUs must not only maximize data acquisition but also minimize energy consumption to ensure cost-effectiveness. Moreover, DCUs must adhere to evolving, location-specific regulations where DCUs are to reduce speed to minimize noise [6]. These decisions introduce additional trade-offs between mission efficiency and regulatory compliance, which must be carefully balanced during planning. Traditional methods struggle with multi-objective adaptation under uncertainty, while conventional DRL approaches often fail to incorporate domain knowledge needed to make economically viable decisions.
 - **Real-Time Decision-Making Under Uncertainty.** Trajectory planning in real-world scenarios requires real-time decision-making across multiple dimensions under dynamic and uncertain conditions, including obstacle avoidance, route selection, and data collection. Traditional optimization methods are often computationally intensive and lack responsiveness, whereas standard DRL policies may require extensive exploration due to task complexity.
- Research gap.** Most existing works have focused on specific aspects of UAV trajectory planning while neglecting others. For instance, [7] and [9]-[13] optimized communication and energy efficiency but did not consider obstacle avoidance. Although [8] and [14] incorporated obstacle avoidance, they were limited to static obstacles and overlooked dynamic threats like other UAVs. Studies using artificial intelligence (AI) techniques, such as [16] and [24], focused on static obstacle avoidance or energy efficiency, yet

> REPLACE THIS LINE WITH YOUR MANUSCRIPT ID NUMBER (DOUBLE-CLICK HERE TO EDIT) <

lacked mechanisms for dynamic obstacle avoidance. Besides, [15], [17]-[23] neglected critical aspects such as obstacle avoidance and adherence to regulatory constraints, limiting their applicability in real-world low-altitude environments.

In summary, existing methods either focus on isolated objectives or assume simplified environments, and thus fail to address all the challenges mentioned above of DCU trajectory planning. To address these limitations, this paper proposes a novel hybrid DRL and large language model (LLM) framework for safe and economical UAV trajectory planning in low-altitude airspace with compliance-awareness. The main contributions are as follows:

- i. We propose a novel UAV trajectory planning system for low-altitude data collection.
- ii. We formulate the problem as a partially observable Markov decision process (POMDP).
- iii. We propose a hybrid SAC and LLM-based trajectory optimization algorithm.

Extensive experiments demonstrate that our proposed method outperforms baseline approaches in terms of data collection rate, collision rate, successful landing rate, regulatory violation rate, energy consumption rate, and yield rate, thereby effectively addressing the three core challenges discussed.

The remainder of this paper is organized as follows. Section II reviews the related work. Section III describes the overall system architecture, while Section IV presents the formal problem definition. Section V introduces the POMDP-based modeling approach and elaborates on the proposed algorithm. Section VI reports the experimental results and performance evaluations. Finally, Section VII concludes the paper and outlines future research directions.

II. RELATED WORK

In this section, we provide related works on planning UAV trajectories using traditional algorithms and AI.

A. UAV Path Planning with Traditional Algorithms

Qin et al. [7] employed a joint optimization algorithm using Dinkelbach's method and block coordinate descent (BCD) to optimize trajectory, power, bit allocation, and phase shift in reconfigurable intelligent surface (RIS)-assisted UAV-enabled mobile edge computing (MEC) systems. Pan et al. [8] proposed a joint UAV power and trajectory optimization framework using an improved non-dominated sorting genetic algorithm-II with K-means initialization operator and variable dimension mechanism (NSGA-II-KV) and an improved particle swarm optimization with normal distribution initialization, genetic mechanism, differential mechanism, and pursuit operator (PSO-NGDP). Pervez et al. [9] studied a multi-UAV MEC system and applied game theory and successive convex approximation (SCA) for joint optimization. Zhang et al. [10] used an elite-driven differential evolution algorithm with dynamic population evolution to jointly optimize UAV deployment and flight planning in Internet of Things (IoT) data collection. Heo et al. [11] incorporated an

NFZ avoidance constraint into UAV trajectory planning and used quadratic transform and SCA for joint optimization. Li et al. [12] applied a swarm intelligence-based algorithm (SIA) to a multi-objective problem involving collaborative beamforming for energy-efficient data harvesting. Fu et al. [13] adopted the distributed approximate Newton (DANE) method and BCD to optimize UAV trajectory, device scheduling, and resource allocation. Wang et al. [14] utilized an ant colony optimization (ACO)-based algorithm for global obstacle avoidance and communication in RIS-assisted UAV systems.

B. UAV Path Planning with AI Algorithms

Silvirianti et al. [15] proposed a layerwise quantum-based DRL (LQ-DRL) method for UAV trajectory planning, user grouping, and power allocation. Liu et al. [16] introduced a local search-based trajectory planning algorithm integrating virtual nodes and tiny machine learning (TinyML) for real-time UAV safety enhancement. Chen et al. [17] formulated a multi-stage mixed-integer nonlinear programming problem and proposed the joint trajectory optimization and resource allocation by DRL for UAV-assisted MEC. Ning et al. [18] addressed distributed trajectory control using DRL and game theory in multi-UAV MEC networks. Song et al. [19] modeled a multi-objective Markov decision process with a trace-based experience replay scheme for energy-efficient UAV trajectory optimization. Ding et al. [20] proposed multi-agent advantage actor-critic with deep deterministic policy gradient (DDPG) and deep attention-based inference (DAI) schemes for spectrum allocation and UAV trajectory design. Wang et al. [21] developed a safe DRL algorithm based on a constrained Markov decision process for UAV trajectory planning. He et al. [22] proposed a distributed multi-objective trajectory design method using distributed DRL for trajectory optimization of multi-UAV. Liu et al. [23] applied multi-agent RL (MARL) and SCA to optimize UAV trajectory in a cell-free space-air-ground integrated network. Ning et al. [24] used constrained DRL to optimize UAV movement and connection assignment in wireless-powered IoT networks.

C. Discussion

Although numerous studies have explored UAV trajectory planning for applications such as data collection, obstacle avoidance remains an under-addressed challenge. For instance, while works [7]–[10] focused on joint optimization of resources and trajectories, they either entirely overlooked obstacle avoidance or considered only static obstacles, failing to address the scenario in the low-altitude airspace. Although [11] incorporated NFZ, it neglected other essential regulatory constraints. Similarly, [12]–[14] did not integrate any obstacle avoidance mechanisms, or again, only addressed static obstacles. Studies [15]–[20] ignored obstacle avoidance altogether, and although [21] introduced learning-based safety mechanisms, it did not jointly consider energy constraints and obstacle avoidance. Furthermore, [22] and [23] omitted obstacle considerations, while [24], like [16], did not account for dynamic obstacles such as other UAVs.

To overcome these challenges, this paper introduces an

> REPLACE THIS LINE WITH YOUR MANUSCRIPT ID NUMBER (DOUBLE-CLICK HERE TO EDIT) <

innovative framework that integrates DRL with LLM to enable safe, compliance-aware, and cost-effective UAV trajectory planning in low-altitude airspace. III. System Description

In this section, we provide a comprehensive description of the system, including the system model and the associated models for UAV mobility, data transmission, and energy consumption. The system model defines the main entities involved, the data collection task, and the underlying system assumptions. The models for mobility, data transmission, and energy consumption characterize the UAV's movement, communication behavior, and energy usage, respectively, in a manner consistent with real-world operations. This modeling approach enhances the credibility of experimental results presented in Section VI. The notations used throughout the remainder of the paper are summarized in TABLE II.

A. System Model

The system model is shown in Fig.1. DCU collects data in \mathbb{A} . Its length, width, and height are X , Y , and Z , respectively.

A.1 System Entity

The system entities include data collection UAV (DCU), other UAVs (OUs), and ground equipment (GE), which are detailed as follows.

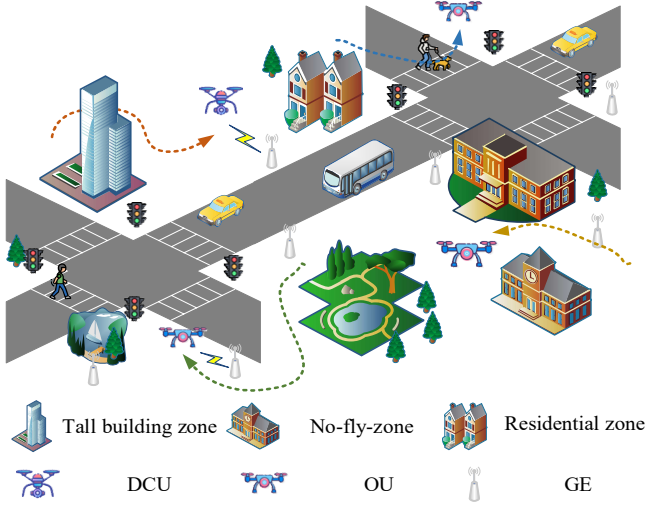


Fig.1 System model.

TABLE II NOTATIONS AND DESCRIPTIONS

Notations	Description
$\mathbb{A} = (X, Y, Z)$	The area, where DCU conducts data collection task, with length X , width Y and height Z .
$\mathbb{T}\mathbb{A} = (p_{\mathbb{T}\mathbb{A}}, l_{\mathbb{T}\mathbb{A}}, w_{\mathbb{T}\mathbb{A}})$	The location of take-off area of DCU with the coordinate point at the lower left corner, the length $l_{\mathbb{T}\mathbb{A}}$, and width $w_{\mathbb{T}\mathbb{A}}$.
$\mathbb{L}\mathbb{A} = (p_{\mathbb{L}\mathbb{A}}, l_{\mathbb{L}\mathbb{A}}, w_{\mathbb{L}\mathbb{A}})$	The location of landing area of DCU.
$\mathbb{R}_{NFZ,l} = (p_{NFZ,l}, l_{NFZ,l}, w_{NFZ,l})$	The location of l -th no-fly zone in \mathbb{A} .
$\mathbb{R}_{RZ,m} = (p_{RZ,m}, l_{RZ,m}, w_{RZ,m})$	The location of m -th residential zone in \mathbb{A} .
$\mathbb{R}_{BZ,n} = (p_{BZ,n}, l_{BZ,n}, w_{BZ,n})$	The location of n -th tall building zone in \mathbb{A} .
N_{NFZ}	The number of no-fly zones.
N_{RZ}	The number of residential zones.

N_{BZ}	The number of tall building zones.
N_{GE}	The number of GEs.
$L_{GE,i} = (x_{GE,i}, y_{GE,i}, 0)$	The location of the i -th GE.
$DV_{GE,i,t}$	The data volume of the i -th GE at time t .
$TP_{GE,i}$	The transmit power of the i -th GE.
N_{OU}	The number of OUs.
$L_{u',j,t} = (x_{u',j,t}, y_{u',j,t}, z_{u',j,t})$	The location of the j -th OU at time t .
$v_{u',j}(t) = (v_{u',j}(t)_x, v_{u',j}(t)_y, v_{u',j}(t)_z)$	The flight speed of the j -th OU at time t .
$L_{u,t} = (x_{u,t}, y_{u,t}, z_{u,t})$	The location of DCU at time t .
$SL = (x_{SL}, y_{SL}, z_{SL})$	The starting location of DCU.
$EL = (x_{EL}, y_{EL}, z_{EL})$	The ending location of DCU.
H	The fixed flight altitude of the UAV.
PR	The perception radius of DCU.
v_{max}	The maximum flight speed of DCU and OUs.
$v_u(t) = (v_u(t)_x, v_u(t)_y, v_u(t)_z)$	The flight speed of DCU at time t .
v_{limit}	The speed limit in \mathbb{R}_{RZ} of DCU.
E_{total}	The total energy that DCU has.
E_{limit}	The maximum energy that DCU can consume in a data collection task.
$E(t)$	The energy consumed by DCU during the time slot Δt .
$e(t)$	The remaining energy of DCU at time t .
$e_{fly}(t)$	The energy consumed of DCU flight during the time slot Δt beginning at time t .
$e_{hover}(t)$	The energy consumed by DCU hovering during the time slot Δt beginning at time t .
Δt	The fixed time slot.
T	The total time for DCU conducting data collection.
t_{fly}	The time used to fly for the time slot Δt .
t_{col}	The time used to collect data for the time slot Δt .
$TD_{u,GE_i}(t)$	The amount of data transmitted between DCU and GE_i for the time slot Δt beginning at time t .
$B_{u,GE_i}(t)$	The effective information rate between DCU and GE_i for the time slot Δt beginning at time t .
$\ CP1 - CP2 / A\ $	The distance between coordinate point 1 and coordinate point 2 or area A .

Data Collection UAV (DCU). DCU is responsible for the data collection task in the low-altitude economy. It takes off from $\mathbb{T}\mathbb{A}$, then conducts data collection in \mathbb{A} , and eventually reaches $\mathbb{L}\mathbb{A}$. When conducting data collection, DCU is not allowed to fly into \mathbb{R}_{NFZ} . Furthermore, when DCU flies to \mathbb{R}_{RZ} , to ensure noise control, its flight speed must be less than v_{limit} [25]. Furthermore, DCU must also ensure that it does not collide with \mathbb{R}_{BZ} and OUs in the low-altitude economic networking. Therefore, we assume that DCU is equipped with a sensing device and the perception radius is PR . Through this device, DCU can know OUs' position and flight direction, and thereby adjust its flight trajectory to avoid collisions.

Other UAVs (OUs). Considering the existence of airspace reuse in the low-altitude economy [26], there will also be OUs performing other tasks in the system. These UAVs may appear

> REPLACE THIS LINE WITH YOUR MANUSCRIPT ID NUMBER (DOUBLE-CLICK HERE TO EDIT) <

on the flight trajectories where DCU collects data. To avoid collisions, the algorithm proposed in this paper will also consider this issue when optimizing DCU flight trajectory.

Ground Equipment (GE). GE is a device that generates data in the low-altitude economy, such as intelligent traffic devices, power infrastructure devices, and environmental monitoring devices [27]. The data generated by GE needs to be collected regularly.

A.2 System Assumptions

The high mobility, dynamic topology, and fast-fading channels cause doppler frequency shift [31], which induces intercarrier interference and raises the bit error rate, thereby degrading DCU data collection performance. Therefore, we use the “hover-and-fly” scheme for DCU [32], and system assumptions about how DCU collects data are as follows:

Assumption 1. We assume that DCU flies at a fixed altitude H . Meanwhile, the maximum flight speed of DCU is v_{\max} while the maximum flight speed of DCU in \mathbb{R}_{RZ} is v_{limit} .

Assumption 2. Given the flight altitude of DCU, the communication link with GE is assumed to follow a line-of-sight channel model [41].

Assumption 3. Both DCU and GE are equipped with a single antenna [33]. The entire data collection period is divided into equal-length time slots ($\{t_i\}_{i=1}^{T/\Delta t}$). In a given time slot Δt , the process is split into two phases: a flight phase, where DCU searches for the optimal communication position, and a data collection phase, where it hovers at that position to collect data.

Assumption 4. DCU collects data from a single randomly selected GE within its communication range in each time slot by using the standard time division multiple access [28].

Assumption 5. DCU connects to GE with the highest received signal power, following a maximum signal strength strategy [41].

B. Models Related to UAV

This section presents models about how UAV moves, transmits data, and consumes energy in our system.

B.1 Mobility Model

The movement model is used to describe how the position of DCU changes at times t and $t+\Delta t$, that is, how DCU moves. Given DCU's position $L_{u,t} = (x_{u,t}, y_{u,t}, z_{u,t})$ and the velocity $v_u(t) = (v_u(t)_x, v_u(t)_y, v_u(t)_z)$ at time t , DCU's position at time $t+\Delta t$ is as follows:

$$L_{u,t+\Delta t} = (x_{u,t} + v_u(t)_x t_{\text{fly}}, y_{u,t} + v_u(t)_y t_{\text{fly}}, z_{u,t} + v_u(t)_z t_{\text{fly}}). \quad (1)$$

According to **Assumptions 1** and **3**, $t_{\text{fly}} = \Delta t / 2$, $z_{u,t} = H$, $v_u(t)_z = 0$, and the distance between $L_{u,t+\Delta t}$ and $L_{u,t}$ should satisfy the following constraint:

$$\|L_{u,t+\Delta t} - L_{u,t}\| \leq v_{\max} t_{\text{fly}}. \quad (2)$$

If DCU flies into \mathbb{R}_{RZ} , the distance between $L_{u,t+\Delta t}$ and $L_{u,t}$ should satisfy the following constraint:

$$\|L_{u,t+\Delta t} - L_{u,t}\| \leq v_{\text{limit}} t_{\text{fly}}. \quad (3)$$

Note that the mobility model of OUs is the same as that of DCU.

B.2 Data Transmission Model

The data transmission model is used to describe how much the data collection volume of DCU changes at times t and $t+\Delta t$, that is, how much data DCU can transmit within time Δt ($TD_{u,GE_i}(t)$). Before giving how to compute $TD_{\Delta t}$, we first present the effective information rate of DCU in the time slot Δt . According to **Assumptions 3** and **4**, when DCU collects data, it is in a hovering state without moving. DCU begins to collect data at time $t+t_{\text{fly}}$ ($t_{\text{fly}} = \Delta t / 2$) and last for $t_{\text{col}} = \Delta t - t_{\text{fly}}$. As a result, assuming the ground device that is currently collecting data is GE_i , the effective information rate during the time slot Δt is as follows:

$$B_{u,GE_i}(t) = \log_2(1 + SNR_{u,GE_i}(t)), \quad (4)$$

where $SNR_{u,GE_i}(t) = TP_{GE_i} G_{u,GE_i}(t) / \mathcal{N}$ is the signal-to-noise ratio in the time slot Δt beginning at time t , TP_{GE_i} is the transmit power of GE_i , $G_{u,GE_i}(t)$ is the channel power gain from DCU to GE_i in the time slot Δt beginning at time t , and \mathcal{N} is the noise power.

According to **Assumption 2**, the free-space path-loss model is used to compute $G_{u,GE_i}(t)$ as follow [34]:

$$G_{u,GE_i}(t) = \frac{\alpha}{\sqrt{\|(x_{u,t+t_{\text{fly}}}, y_{u,t+t_{\text{fly}}}, H) - (x_{GE_i}, y_{GE_i}, 0)\|^2}}, \quad (5)$$

where α is the channel power gain at $\sqrt{\|(x_{u,t+t_{\text{fly}}}, y_{u,t+t_{\text{fly}}}, H) - (x_{GE_i}, y_{GE_i}, 0)\|^2} = 1$ m distance.

Note that, if DCU wants to transmit data, $SNR_{u,GE_i}(t)$ must exceeds a certain threshold τ [35]. Therefore, according to Equations (4) and (5), $TD_{u,GE_i}(t)$ can be computed as follows:

$$TD_{u,GE_i}(t) = \begin{cases} B_{u,GE_i}(t)\Delta t, & \text{if } DV_{GE_i,t} > B_{u,GE_i}(t) \text{ and } SNR_{u,GE_i}(t) \geq \tau, \\ DV_{GE_i,t}, & \text{if } DV_{GE_i,t} \leq B_{u,GE_i}(t) \text{ and } SNR_{u,GE_i}(t) \geq \tau, \\ 0, & SNR_{u,GE_i}(t) < \tau_s. \end{cases} \quad (6)$$

B.3 Energy Consumption Model

The energy consumption model is used to describe how much the remaining energy of DCU changes at times t and $t+\Delta t$, that is, how much energy DCU consumes within time Δt ($E(t)$). According to **Assumption 3**, the energy consumption of DCU within Δt beginning at time t can be divided into two parts: $e_{\text{fly}}(t)$ and $e_{\text{hover}}(t)$. For $e_{\text{fly}}(t)$, it can be computed as follows [37]:

> REPLACE THIS LINE WITH YOUR MANUSCRIPT ID NUMBER (DOUBLE-CLICK HERE TO EDIT) <

$$e_{fly}(t) = (\lambda / 8 \cdot \rho \eta A_r \mathfrak{S}^3 r_{rotor}^3 \left(1 + \frac{3v_u(t)^2}{U_{tip}^2} \right) + \frac{1}{2} d_0 \rho S A_r v_u(t)^3) t_{fly}, \quad (7)$$

where λ denotes the profile drag coefficient, A_r the rotor disc area, \mathfrak{S} the blade angular velocity, r_{rotor} the rotor radius, d_0 denotes the fuselage drag coefficient, ρ the density of air, η the rotor solidity factor, U_{tip} the tip velocity of the rotor blade, λ the average induced velocity during hovering, v_u the velocity of DCU.

For $e_{hover}(t)$, it can be computed as follows:

$$e_{hover}(t) = ((1 + \mathfrak{R})w)^{3/2} \sqrt{1 + \frac{v_u(t)^4}{4v_0^4} - \frac{v_u(t)^2}{2v_0}} / \sqrt{2\rho A_r} t_{hover}, \quad (8)$$

where \mathfrak{R} is the incremental correction factor to induced power, w the weight of DCU, v_0 the mean rotor induced velocity in hover. Note that since the energy consumed by DCU for communication is much less than that consumed for hovering [36], when calculating $e_{hover}(t)$, we ignore the energy consumed by DCU for data transmission. Besides, the UAV-related parameter values in this section follow the settings provided in [37].

IV. OPTIMIZATION PROBLEM

In this section, we present the main requirements behind the optimization problem to highlight the motivation before formally defining it.

A. Requirement Analysis

The optimization problem involves two primary requirements. First are the objective constraints imposed by the physical environment, and second are the task-specific requirements associated with data collection in the low-altitude economy. For the former, the following requirements are taken into considered:

R1) Limited mobility. The moving distance of DCU during each time slot should satisfy the Equation (2).

For the latter, the following requirements are taken into considered:

R2) Robust obstacle avoidance. Since data collection in the low-altitude economy is concentrated in urban areas and there is airspace reuse in low-altitude areas, when DCU conducts data collection, it not only needs to avoid \mathbb{R}_{BZ} , \mathbb{R}_{NFZ} but also OUs.

R3) Compliance. Unlike general data collection tasks, DCUs operating in urban low-altitude environments must comply with strict regulations. They must reduce speed near \mathbb{R}_{BZ} to minimize noise and meet regulatory standards.

R4) Economy. Within the low-altitude economy, data collection tasks must jointly consider the maximization of data acquisition and the minimization of energy consumption to maximize the data collection task benefits. Consequently,

DCU is required not only to collect sufficient data but also to complete the task along an energy-efficient, near-optimal trajectory that minimizes travel distance and associated energy costs.

B. Problem Formulation

According to the requirement analysis introduced in Section IV.A, we try to optimize the flight trajectory of DCU while maximizing the amount of collected data. The optimization problem can be formally formulated as follows:

$$OP : \arg \max \sum_{t=0}^T TD_{u,GE_i}(t), \quad (8)$$

s.t.

$$GE_i = \arg \max(\{B_{u,GE_i}(t)\}_{i=1}^{N_{GE}} \wedge SNR_{u,GE_i}(t) \geq \tau) \quad (8a)$$

$$t+1 = t + \Delta t, \forall t \quad (8b)$$

$$L_{u,t+1} = (x_{u,t} + v_u(t)_x t_{fly}, y_{u,t} + v_u(t)_y t_{fly}, z_{u,t}) \quad (8c)$$

$$v_u(t) \leq v_{max}, \forall t \quad (8d)$$

$$v_u(t) \leq v_{limit}, \text{ if } L_{u,t} \in \{\mathbb{R}_{RZ,m}\}_{m=1}^{N_{RZ}} \quad (8e)$$

$$(L_{u,t}, L_{u',t} \in \mathbb{A}) \forall t \quad (8f)$$

$$(L_{u,t}, L_{u',t} \notin \{\mathbb{R}_{BZ,n}\}_{n=1}^{N_{BZ}}) \wedge (L_{u,t}, L_{u',t} \notin \{\mathbb{R}_{NFZ,l}\}_{l=1}^{N_{NFZ}}), \forall t \quad (8g)$$

$$\|L_{u,t} - L_{u',t}\| > 0, \forall t, j(j \in [1, N_U]) \quad (8h)$$

$$\sum_{t=0}^T (e_{fly}(t) + e_{hover}(t)) \leq E_{limit} \quad (8i)$$

The objective function OP maximizes the amount of data collected over the given time slots. Constraint (8a) selects GE to collect data according **Assumption 5**, while (8b) presents the relationship between t and $t+1$ according to the data transmission model. Constraint (8c) governs the position updates of DCU according the mobility model. According **Assumption 1** Constraint (8d) enforces the maximum speed limit, and Constraint (8e) enforces the maximum speed limit in \mathbb{R}_{RZ} to satisfy **R1** and **R3**. Constraints (8f), (8g), and (8h) ensure that DCU operates within \mathbb{A} , avoids \mathbb{R}_{NFZ} , and prevents collisions with \mathbb{R}_{BZ} or OUs to satisfy **R2** and **R3**. Constraint (8i) ensures the maximum energy consumption of DCU in a data collection task to satisfy **R4**.

V. OUR ALGORITHM FOR PATH PLANNING

This section first formulates the optimization problem from Section IV as a POMDP to enable solution via DRL. We then present SAC algorithm, which serves as the foundation for our algorithm. Finally, we introduce the proposed algorithm and demonstrate its effectiveness in addressing the formulated problem.

A. POMDP Modeling

As the future position of DCU is determined solely by its current state (i.e., position and velocity), the path planning problem satisfies the Markov property. Nevertheless, due to DCU's limited ability to perceive the full environmental state, the problem is more appropriately formulated as a POMDP, defined by a corresponding tuple $(\mathcal{O}, \mathcal{A}, r, \mathcal{P}, \delta)$, where the

> REPLACE THIS LINE WITH YOUR MANUSCRIPT ID NUMBER (DOUBLE-CLICK HERE TO EDIT) <

observation space \mathcal{O} replaces the state space [38]. Then, the details of \mathcal{O}, \mathcal{A} , and r in $(\mathcal{O}, \mathcal{A}, r, \mathcal{P}, \delta)$ are as follows:

Observation Space \mathcal{O} : $o_t (o_t \in \mathcal{O})$ is the state that DCU can observe at time t , where $o_t = (o_{GE,t}, o_{Z,t}, o_{u,t}, o_{u,t})$.

- $o_{GE,t}$ is the state about all GEs and $o_{GE,t} = \{L_{GE,i}, DV_{GE,i}, TP_{GE,i}\}_{i=1}^{N_{GE}}$.
- $o_{Z,t}$ is the state about all zones and $o_{Z,t} = \{\{\mathbb{R}_{NFZ,l}\}_{l=1}^{N_{NFZ}}, \{\mathbb{R}_{RZ,m}\}_{m=1}^{N_{RZ}}, \{\mathbb{R}_{BZ,n}\}_{n=1}^{N_{BZ}}\}$.
- $o_{u,t}$ is the state about all OUs and $o_{u,t} = \{L_{u',t}, v_{u',t}\}_{j=1}^{N_{U'}}$.
- $o_{u,t}$ is the state about DCU itself and $o_{u,t} = \{L_{u,t}, v_{u,t}, E(t), TD_{u,GE_i}(t), \mathbb{T}\mathbb{A}, \mathbb{L}\mathbb{A}\}$.

Action Space \mathcal{A} : $a_t (a_t \in \mathcal{A})$ is the sampled action at time t and $a_t = (v(t)_x, v(t)_y, 0)$, which means DCU will move at the velocity $(v_x(t), v_y(t), 0)$ at time t .

Reward function r : r is used to effectively guide the path planning during the data collection process and plays a critical role in both the efficiency and performance of policy learning. To facilitate learning an optimal policy aligned with the objective function OP and its associated constraints, we formulate a composite reward function, expressed as follows:

$$r_t = r_{1t} + r_{2t} + r_{3t} + r_{4t} + r_{5t} + r_{6t} + r_{7t} + r_{8t} + r_{9t}. \quad (20)$$

r_{1t} encourage DCU to collect data and is as follows:

$$r_{1t} = \begin{cases} \sigma_1, & \text{if } TD_{u,GE_i}(t+1) \geq 0, \\ 0, & \text{otherwise.} \end{cases} \quad (21)$$

r_{2t} is used to ensure that DCU will not collide with OUs and is as follows:

$$r_{2t} = \begin{cases} 0, & \text{if } d_{t,u'} \geq d_{safe,u'}, \\ -\sigma_2 \times \frac{d_{safe,u'} - d_{t,u'}}{d_{safe,u'} - d_{min,u'}}, & \text{if } d_{min,u'} < d_{t,u'} < d_{safe,u'}, \\ -\sigma_2, & \text{if } d_{t,u'} \leq d_{min,u'}, \end{cases} \quad (22)$$

where $d_{t,u'} = \text{argmin}\{\|L_{u,t} - L_{u',t}\|\}_{j=1}^{N_{U'}}$, $d_{min,u'}$ is the minimum safe distance between DCU and OUs, which is used for DCU to adjust the speed to avoid collisions, and, $d_{safe,u'}$ is the safe distance threshold between DCU and OUs.

r_{3t} is used to ensure that DCU will not collide with tall buildings and is as follows:

$$r_{3t} = \begin{cases} 0, & \text{if } d_{t,BZ} \geq d_{safe,BZ}, \\ -\sigma_3 \times \frac{d_{safe,BZ} - d_{t,BZ}}{d_{safe,BZ} - d_{min,BZ}}, & \text{if } d_{min,BZ} < d_{t,BZ} < d_{safe,BZ}, \\ -\sigma_3, & \text{if } d_{t,BZ} \leq d_{min,BZ}, \end{cases} \quad (23)$$

where $d_{t,BZ} = \text{argmin}\{\|L_{u,t} - \mathbb{R}_{BZ,n}\|\}_{n=1}^{N_{BZ}}$, $d_{min,BZ}$ is the minimum safe distance between DCU and tall buildings, which is used for DCU to adjust the speed to avoid collisions,

and, $d_{safe,BZ}$ is the safe distance threshold between DCU and tall buildings.

r_{4t} is used to ensure that DCU will not fly into NFZs and is as follows:

$$r_{4t} = \begin{cases} 0, & \text{if } d_{t,NFZ} \geq d_{safe,NFZ}, \\ -\sigma_4 \times \frac{d_{safe,NFZ} - d_{t,NFZ}}{d_{safe,NFZ} - d_{min,NFZ}}, & \text{if } d_{min,NFZ} < d_{t,NFZ} < d_{safe,NFZ}, \\ -\sigma_4, & \text{if } d_{t,NFZ} \leq d_{min,NFZ}, \end{cases} \quad (24)$$

where $d_{t,NFZ} = \text{argmin}\{\|L_{u,t} - \mathbb{R}_{NFZ,l}\|\}_{l=1}^{N_{NFZ}}$, $d_{min,NFZ}$ is the minimum safe distance between DCU and NFZs, which is used for DCU to adjust the speed to avoid collisions, and, $d_{safe,NFZ}$ is the safe distance threshold between DCU and NFZs.

r_{5t} is used to ensure that the speed of DCU when flying into residential areas meets the speed limit and is as follows:

$$r_{5t} = \begin{cases} 0, & \text{if } v_u(t) \leq v_{limit}, L_{u,t} \in \{\mathbb{R}_{RZ,m}\}_{m=1}^{N_{RZ}}, \\ -\sigma_5 \times \frac{v_u(t) - v_{limit}}{v_{max} - v_{limit}}, & \text{if } v_{limit} < v_u(t) \leq v_{max}, L_{u,t} \in \{\mathbb{R}_{RZ,m}\}_{m=1}^{N_{RZ}}. \end{cases} \quad (25)$$

r_{6t} is used to ensure that DCU should not fly out of the given area and is as follows:

$$r_{6t} = \begin{cases} 0, & \text{if } d_{t,\mathbb{A}} \geq d_{safe,\mathbb{A}}, \\ -\sigma_6 \times \frac{d_{safe,\mathbb{A}} - d_{t,\mathbb{A}}}{d_{safe,\mathbb{A}} - d_{min,\mathbb{A}}}, & \text{if } d_{min,\mathbb{A}} < d_{t,\mathbb{A}} < d_{safe,\mathbb{A}}, \\ -\sigma_6, & \text{if } L_{u,t} \notin \mathbb{A}, \end{cases} \quad (26)$$

where $d_{t,\mathbb{A}} = \|L_{u,t} - \mathbb{A}\|$ is the distance between DCU and the boundary of \mathbb{A} at time t , $d_{min,\mathbb{A}}$ is the minimum safe distance between DCU and the boundary of \mathbb{A} , which is used for DCU to adjust the speed to avoid flying out, and, $d_{safe,\mathbb{A}}$ is the safe distance threshold between DCU and the boundary of \mathbb{A} .

r_{7t} is used to encourage that DCU can land within the landing area and is as follows:

$$r_{7t} = \begin{cases} 0, & \text{if } d_{t,\mathbb{L}\mathbb{A}} \geq d_{tar,\mathbb{L}\mathbb{A}}, \\ -\sigma_7 \times (1 - \frac{d_{t,\mathbb{L}\mathbb{A}}}{d_{tar,\mathbb{L}\mathbb{A}}}), & \text{if } 0 < d_{t,\mathbb{L}\mathbb{A}} < d_{tar,\mathbb{L}\mathbb{A}}, \end{cases} \quad (27)$$

r_{8t} is used to encourage that DCU returns to the landing area before its energy is exhausted and is as follows:

$$r_{8t} = \begin{cases} 0, & \text{if } e(t) \geq e_{min}(t), \\ -\sigma_8 \times \frac{e_{min}(t) - e(t)}{e_{min}(t)}, & \text{if } e(t) < e_{min}(t), \end{cases} \quad (28)$$

where $e_{min}(t) = e_{fy}(t) d_{t,\mathbb{L}\mathbb{A}} / v_{max}$.

r_{9t} is used to encourage DCU can complete the data collection task quickly to reduce energy consumption and is as

> REPLACE THIS LINE WITH YOUR MANUSCRIPT ID NUMBER (DOUBLE-CLICK HERE TO EDIT) <

follows:

$$r_{9t} = -\sigma_9 \quad (29)$$

B. SAC Algorithm

SAC is a state-of-the-art off-policy DRL algorithm based on the maximum entropy framework [29]. Its off-policy nature allows flexible integration of external guidance from LLMs without compromising training stability or policy optimization efficiency. Additionally, SAC is well-suited for our problem, which involves a continuous action space. Although we adopt SAC in this study, we believe that other off-policy DRL algorithms supporting continuous action spaces may also achieve comparable performance.

The maximum entropy DRL incorporates the policy's entropy into the objective function [30], modifying the learning goal as follows:

$$\pi^* = \arg \max_{\pi} \sum_{t=0}^{\infty} E_{\mathcal{P}_{\pi}} [\delta^t (r_t + \mu P(\pi(\cdot | o_t)))], \quad (9)$$

where δ is the discounted factor and μ is the temperature parameter. The policy entropy $P(x)$ is defined as follows:

$$P(x) = -\sum_x p(x) \log p(x), \quad (10)$$

Given the soft value-state function and the soft value function as follows:

$$Q_{soft}(o_t, a_t) = r_t + E_{\mathcal{P}_{\pi}} [\sum_{i=1}^{\infty} \delta^i (r_{t+i} + \mu P(\cdot | \pi))], \quad (11)$$

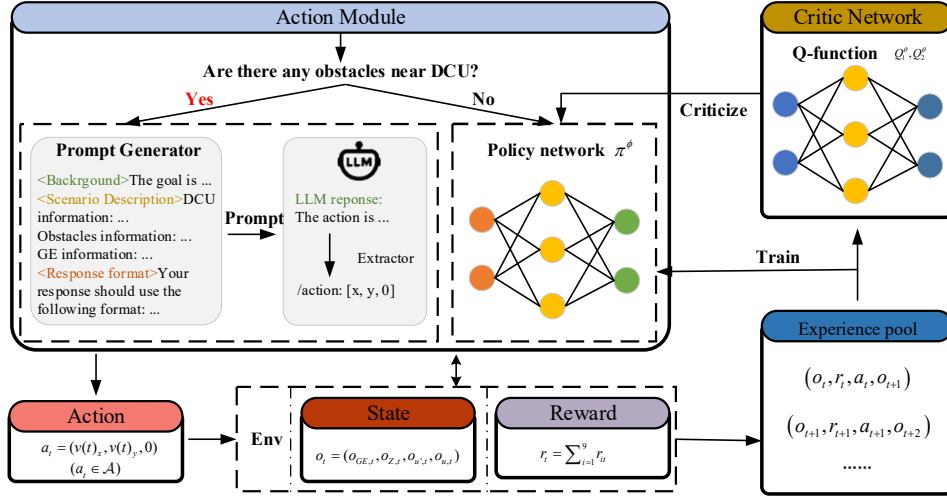


Fig.2 The main process of our algorithm.

where \tilde{a}_{t+1} denotes the next action sampled from the policy given the next state o_{t+1} .

For π , with the sampled action, it is optimized as follows:

$$J_{\pi}(\phi) = E_{\substack{o_t \sim D \\ \zeta \sim N}} [\beta \log \pi^{\phi}(\tilde{a}_t^{\phi}(o_t, \zeta) | o_t) - \min_{j=1,2} Q_j^{\phi}(o_t, \tilde{a}_t^{\phi}(o_t, \zeta))], \quad (18)$$

where $\tilde{a}_t^{\phi}(o_t, \zeta)$ is as follows:

$$\tilde{a}_t^{\phi}(o_t, \zeta) = \tanh(\beta^{\phi}(o_t) + \alpha^{\phi}(o_t) \odot \zeta), \zeta \sim N(0,1), \quad (19)$$

where β and α represent the mean and standard deviation of the Gaussian distribution, respectively; ζ denotes the noise; and $N(0,1)$ indicates the standard normal distribution.

$$V_{soft}(o_t) = \mu \log \int_{\mathcal{A}} \exp(Q_{soft}(o_t, a') / \mu) da'. \quad (12)$$

They can be iterated in the following ways:

$$Q_{soft}(o_t, a_t) = r_t + \delta E_{\mathcal{P}} [V_{soft}(o_{t+1})], \quad (13)$$

$$V_{soft}(o_t) = E_{\pi} [Q_{soft}(o_t, a_t) - \mu \log \pi(a_t | o_t)]. \quad (14)$$

Therefore, the policy π is as follows:

$$\pi(o_t, a_t) = \exp(Q_{soft}(o_t, a_t) / \delta - V_{soft}(o_t)). \quad (15)$$

In SAC, both π and Q_{soft} are parameterized using neural networks. This enables SAC to handle continuous state and action spaces, making it well-suited for solving complex problems and enhancing controller performance in the scenario, such as path planning. The neural networks associated with Q_{soft} are updated at each step by minimizing the following loss function:

$$J_Q(\phi) = E_{(o_t, a_t, r_t, o_{t+1}, \zeta \sim D)} [(Q_j^{\phi}(o_t, a_t) - y(r_t, o_{t+1}))^2], \quad (16)$$

where $y(r_t, o_{t+1})$ is as follows:

$$y(r_t, o_{t+1}) = r_t + \delta (\min_{j=1,2} Q_j^{\phi}(o_{t+1}, \tilde{a}_{t+1}) - u \log \pi^{\phi}(\tilde{a}_{t+1} | o_{t+1})), \quad (17)$$

C. Our Algorithm

This section details the main idea about how we construct our path planning algorithm and the algorithm itself.

C.1 Main Idea

Based on the POMDP formulated in Section V.B, and considering that the velocity of DCU is a continuous variable, we adopt SAC algorithm to optimize the flight trajectory of DCU during the data collection process. Furthermore, in light of the regulatory constraints and high obstacle-avoidance demands in low-altitude economy scenarios, we propose enhancing the SAC framework by integrating LLM into the action selection mechanism. Specifically, under certain

> REPLACE THIS LINE WITH YOUR MANUSCRIPT ID NUMBER (DOUBLE-CLICK HERE TO EDIT) <

conditions, LLM can substitute the policy network to determine DCU’s action based on the current state.

Given LLM’s rich prior knowledge, we employ it for decision-making when DCU encounters obstacle-avoidance scenarios—for instance, when obstacles such as buildings, NFZs, or OUs appear within its observation range. In such cases, LLM is invoked to guide DCU in selecting feasible and regulation-compliant actions.

C.2 Algorithm Detail

Our proposed algorithm, which are detailed in **Algorithm 1**, is designed to enable DCU to effectively perform data collection by learning an optimal velocity control policy that guides its trajectory to maximize data acquisition and avoid collision. The main process of our algorithm is shown in Fig.2.

Algorithm 1 SAC with LLM-based Path Planning Algorithm

```

Input: The environment  $E$  1
Output: The optimal policy network  $\pi^*$  2
Initialize: Q-function parameters  $\theta_1, \theta_2$ , policy parameter  $\phi$ , and LLM, 3
experience pool  $D$ , target parameters  $\theta_{1, tar}, \theta_{2, tar}$  4
For  $episode = 1, 2, \dots, L$  do: 5
  Initialize  $E$ :  $E \leftarrow EnvReset()$  6
  For each  $step = 1, 2, \dots, N$  do: 7
    Observe state:  $o_t \leftarrow ObsState(E)$  8
    Judge if using LLM or not:  $bool \leftarrow useLLM(\tilde{o}_t)$  9
    If bool: 10
      Select action from LLM:  $a_t \leftarrow LLM(\tilde{o}_t)$  11
    Else 12
      Select action from policy network:  $a_t \leftarrow \pi^\phi(o_t)$  13
    Execute action and get new state, reward:  $(o_{t+1}, r_t, done) \leftarrow ExeAct(a_t)$  14
    Store state, action and reward in experience pool:  $(o_t, r_t, a_t, o_{t+1}) \rightarrow D$  15
    If  $done$ , reset the environment and continue 16
  End for 17
For each gradient step do: 18
  Randomly sample a batch of samples:  $(o_t, r_t, a_t, o_{t+1}) \leftarrow D$  19
  Compute targets and update Q-functions:  $Q_1^o, Q_2^o$  20
  Update policy network  $\pi^\phi$  21
  Update target parameters:  $\theta_{1, tar}, \theta_{2, tar}$  22
End for 23

```

The proposed algorithm takes the environment as input (**Line 1**) and outputs an optimal policy network (**Line 2**) that governs the velocity control of DCU. Upon initialization (**Line 3**), the initialization of the Q-function parameters, policy network parameters, LLM, the experience pool, and the target network parameters is conducted.

For each training episode, the environment is first reset (**Line 5**). Then, at each time step within the episode, the algorithm observes the current state and determines whether to invoke LLM for action selection (**Lines 7, 8**). It is important to note that this state (\tilde{o}_t) differs from the state (o_t) used by the policy network. Specifically, it refers to the pre-processed, semantically rich environmental information, such as the positions of obstacles within DCU’s observation range, as illustrated in Fig.2. If the decision condition is met, LLM is utilized to select an action for DCU based on this semantic

state information. Otherwise, the action is selected using the policy network (**Lines 9-12**). The selected action is then executed, resulting in the next state and corresponding reward for the subsequent time slot. Simultaneously, the current state, action, and reward are stored in the experience pool (**Lines 13, 14**). The algorithm then checks whether the current episode has terminated. If so, it proceeds to the next episode (**Line 15**).

For each gradient update step, a batch of samples is drawn from the experience pool (**Line 18**). Based on this batch, the target values are computed, and the Q-function, policy network, and target network parameters are updated accordingly (**Lines 19-21**). This process repeats until the episode concludes, after which the next episode begins. Upon completion of all training episodes, the algorithm outputs the final optimized policy network.

VI. EXPERIMENT

In this section, we present the experimental results of the proposed algorithm. Prior to that, we describe the experimental setup and evaluation metrics.

A. Experiment Setting

For the hardware, all experiments in this study were conducted on a computing platform equipped with Intel® Xeon® Gold 6230 CPUs and NVIDIA GeForce RTX 4090 GPUs.

TABLE III ENVIRONMENT PARAMETERS SETTING

Para.	Value	Para.	Value	Para.	Value
N_{GE}	[11, 15]	v_{max}	10 m/s	\mathcal{N}	10e-6
DV_{GE_i}	[1, 3]	v_{limit}	5 m/s	PR	20 m
TP_{GE_i}	0.01 w	E_{total}	1e6 J	d_{min}, d_{safe}	5 m, 15 m
$N_{U'}$	[3, 7]	E_{limit}	8e5 J	τ	3.6

A.1 Environment Parameters

According to **Assumption 1**, the experimental environment is simplified to a two-dimensional space with \mathbb{A} of 500 m in both length and width. \mathbb{TA} and \mathbb{LA} are square regions measuring 25×25 m, located at the top-left and bottom-right corners of \mathbb{A} , respectively. Given the urban deployment scenario, the environment includes rectangular \mathbb{R}_{NFZ} , \mathbb{R}_{RZ} , and \mathbb{R}_{BZ} with the range of [50, 200] m for both length and width. The number of are randomly chosen from the range [1, 3]. The weights assigned to the components of the reward function are set to [8, 0.4, 0.4, 0.4, 0.6, 0.4, 0.6, 1, 0.01] and can be flexibly adjusted to reflect different task priorities. Other environmental parameters are detailed in TABLE III.

TABLE IV HYPERPARAMETERS SETTING

Para.	Value
Learning rate of actor network	0.0001
Learning rate of critic network	0.0003
Number of episodes	4000
Clip range	0.2
Batch size	256
Discount factor	0.99
Number of hidden layers of DNNs	2
Hidden layer size	64

> REPLACE THIS LINE WITH YOUR MANUSCRIPT ID NUMBER (DOUBLE-CLICK HERE TO EDIT) <

A.2 Algorithm Parameters

For the algorithm, hyperparameters used by the proposed algorithm and other baselines are shown in TABLE IV. For LLM used in our algorithm, we choose the DeepSeek-R1 [39].

B. Evaluation Metrics

For the metrics used to evaluate the proposed algorithm and other baselines, we use the following metrics that used by the general UAV data collection flight trajectory optimization tasks [40]. Assuming N_{total} is the number of experiment test.

- **Data collection rate:** This metric quantifies the ratio average of successfully collected data by DCU relative to the total target data volume in N_{total} data collection tasks, which can be computed as follows:

$$DCR = \sum_{i=1}^{N_{test}} D_{DCU,i} / \sum_{i=1}^{N_{test}} D_{total,i}, \quad (30)$$

where $D_{DCU,i}$ is the collected data volume by DCU and $D_{total,i}$ is the total target data volume in one task.

- **Collision rate:** This metric quantifies the ratio of data collection tasks in which DCU collides with OUs, \mathbb{R}_{BZ} , or flies into \mathbb{R}_{NFZ} relative to the total number of tasks, which can be computed as follows:

$$CR = N_C / N_{total}, \quad (31)$$

where N_C is the number of tasks in which DCU collides with OUs, \mathbb{R}_{BZ} , or flies into \mathbb{R}_{NFZ} .

- **Successful landing rate:** This metric quantifies the ratio of data collection tasks in which DCU can returns to $\mathbb{L}\mathbb{A}$ before depleting its energy, which can be computed as follows:

$$SLR = N_{SLR} / N_{total}, \quad (32)$$

where N_{SLR} is the number of tasks in which DCU can returns to $\mathbb{L}\mathbb{A}$ before depleting its energy.

In addition to the commonly used metrics mentioned above, the following indicators are also employed to evaluate the effectiveness of satisfying the requirement for data collection trajectory optimization under the low-altitude economy.

- **Regulatory violation rate:** This metric quantifies the ratio of data collection tasks in which DCU exceeds speed limits within \mathbb{R}_{RZ} , which can be computed as follows:

$$RVR = N_{RVL} / N_{total}, \quad (33)$$

where N_{RVL} is the number of tasks in which DCU exceeds speed limits within \mathbb{R}_{RZ} .

- **Energy consumption rate:** This metric quantifies the ratio average of energy consumed by DCU relative to the total energy in N_{total} data collection tasks, which can be computed as follows:

$$ECR = \sum_{i=1}^{N_{test}} E_{EVR,i} / \sum_{i=1}^{N_{test}} E_{total,i}, \quad (34)$$

where $E_{EVR,i}$ is the energy consumed by DCU and $E_{total,i}$ is the total energy in one task.

- **Yield rate:** This metric quantifies the ratio of data collection tasks in which the energy consumed by DCU remains below E_{limit} , which can be computed as follows:

$$YR = N_{YR} / N_{total}, \quad (35)$$

where N_{YR} is the number of tasks in which the energy consumed by DCU remains below E_{limit} .

C. Experiment Results

In this section, we present a comparative analysis between the proposed algorithm and several baseline methods in terms of UAV flight trajectories and metrics mentioned above. The baselines are as follows:

- **Heuristic Algorithm:** A rule-based strategy is used to determine the actions of DCU for data acquisition and obstacle avoidance. DCU sequentially collects data from the nearest GE until all data is acquired. If a static obstacle such as \mathbb{R}_{NFZ} or \mathbb{R}_{BZ} is encountered, DCU performs detouring maneuvers. For dynamic obstacles like OUs, it either hovers in place or retreats to avoid collision until OU moves away. When flying over \mathbb{R}_{RZ} , DCU reduces its speed to comply with regulations. Furthermore, if the remaining energy is only sufficient for returning to $\mathbb{L}\mathbb{A}$, DCU will immediately head back.
- **LLM-based Method:** An LLM, DeepSeek-R1, is used in real-time to decide the actions of DCU. We provide LLM with the state information within a 100-meter radius around DCU, as well as the positions of the two nearest GEs. In addition, we also provide the LLM with E_{limit} of DCU.
- **SAC+LLM:** SAC is used during training, with a certain probability of delegating action selection to LLM instead of the policy network. LLM used here is the same as the one employed in the proposed algorithm, i.e., DeepSeek-R1.
- **SAC:** A pure DRL approach using the SAC without LLM integration.

C.1 Flight Trajectories about Baselines and Our Algorithm

Before presenting the flight trajectories, we first provide the training reward curves for baselines and the proposed algorithm. The training reward curves, as illustrated in Fig.3, demonstrate the convergence behavior of various algorithms across 4000 episodes. It can be observed that both the proposed algorithm and SAC achieve convergence over time. However, the proposed method consistently attains a significantly higher reward at convergence, indicating superior policy quality and more effective data collection strategies. In contrast, the variants that combine SAC with LLM, where LLM is invoked with a fixed probability (0.3, 0.4, or 0.5) to select actions, fail to converge to an optimal policy. These approaches exhibit lower and more volatile reward trajectories throughout training. This instability suggests that the random delegation of action selection to LLM disrupts the learning dynamics of SAC, resulting in suboptimal performance. The superior performance of the proposed algorithm underscores the effectiveness of its selective invocation strategy, wherein LLM is engaged specifically for obstacle avoidance decisions.

> REPLACE THIS LINE WITH YOUR MANUSCRIPT ID NUMBER (DOUBLE-CLICK HERE TO EDIT) <

This targeted use of LLM not only preserves the stability of SAC’s policy learning but also leverages LLM’s strengths in high-level decision-making scenarios. The results validate the design choice of integrating LLM in a context-aware manner, rather than applying it indiscriminately during training.

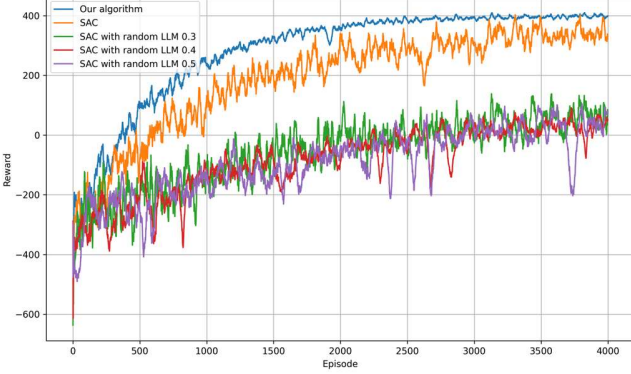
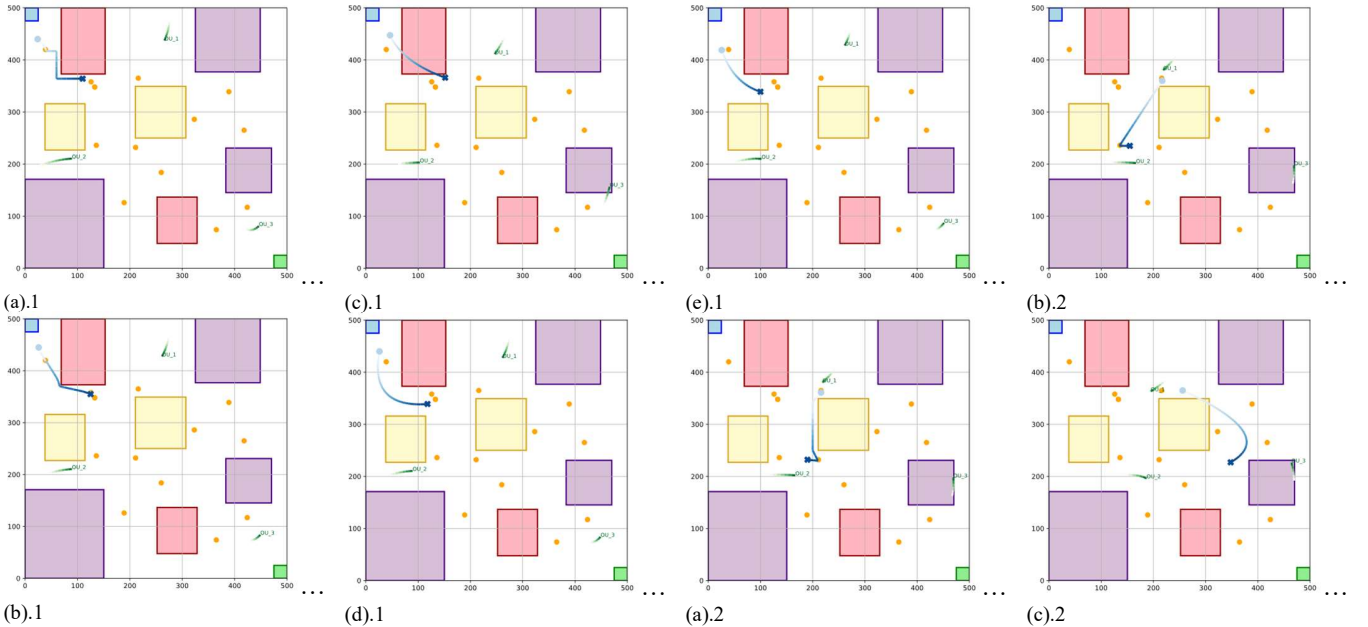


Fig.3 Training reward curves about baselines and our algorithm.

Fig.4 illustrates segments of DCU’s flight trajectories during data collection under both the proposed algorithm and the baseline methods. We highlight four typical stages: static obstacle avoidance, data collection paths, dynamic obstacle avoidance, and return to the landing zone.

Figs.4.(a).1 and (b).1 illustrate that both the heuristic and the LLM-based approaches predominantly follow a “nearest GE” strategy for data collection. However, the LLM-based approach exhibits more efficient path planning, demonstrating a tendency to select shorter and more obstacle-aware trajectories. Notably, Fig.4.(b).2 indicates that LLM does not rigidly adhere to the nearest GE principle; instead, it appears

to balance the trade-off between obstacle avoidance and data acquisition efficiency. Despite this, as shown in Figs.4.(a).4 and (b).4, adherence to the nearest GE strategy tends to increase the overall flight distance. As a result, both the heuristic and LLM-based approaches often encounter a scenario where DCU reaches its energy limit before completing the data collection task, thereby necessitating an early return to $\mathbb{L}\mathbb{A}$. Fig.4.(c) presents the performance of the SAC+LLM approach, wherein LLM is stochastically invoked during training to determine DCU’s actions. This integration does not effectively enhance SAC’s decision-making capability and, in fact, leads to performance degradation. As observed in Figs.4.(c).1 and (c).4, this method results in suboptimal obstacle avoidance and frequently prevents DCU from successfully returning to $\mathbb{L}\mathbb{A}$, often exhausting its energy mid-flight. Fig.4.(d) and (e) depict the flight trajectories generated by the SAC algorithm and the proposed method, respectively. From Figs.4.(d).1 and (e).1, it can be observed that SAC adopts a more conservative obstacle avoidance strategy, which inadvertently increases flight distance. Figs.4.(d).2 and (e).2 show that SAC may overlook distant GEs, resulting in reduced data acquisition. Furthermore, Figs.4.(d).3 and (e).3 indicate that SAC tends to forgo data collection opportunities in the presence of obstacles, adversely affecting overall data completeness. Finally, Figs.4.(d).4 and (e).4 reveal that SAC may opt to traverse residential areas directly. Empirical testing suggests that SAC occasionally exceeds speed limits within these zones, thereby compromising compliance with operational regulations.



> REPLACE THIS LINE WITH YOUR MANUSCRIPT ID NUMBER (DOUBLE-CLICK HERE TO EDIT) <

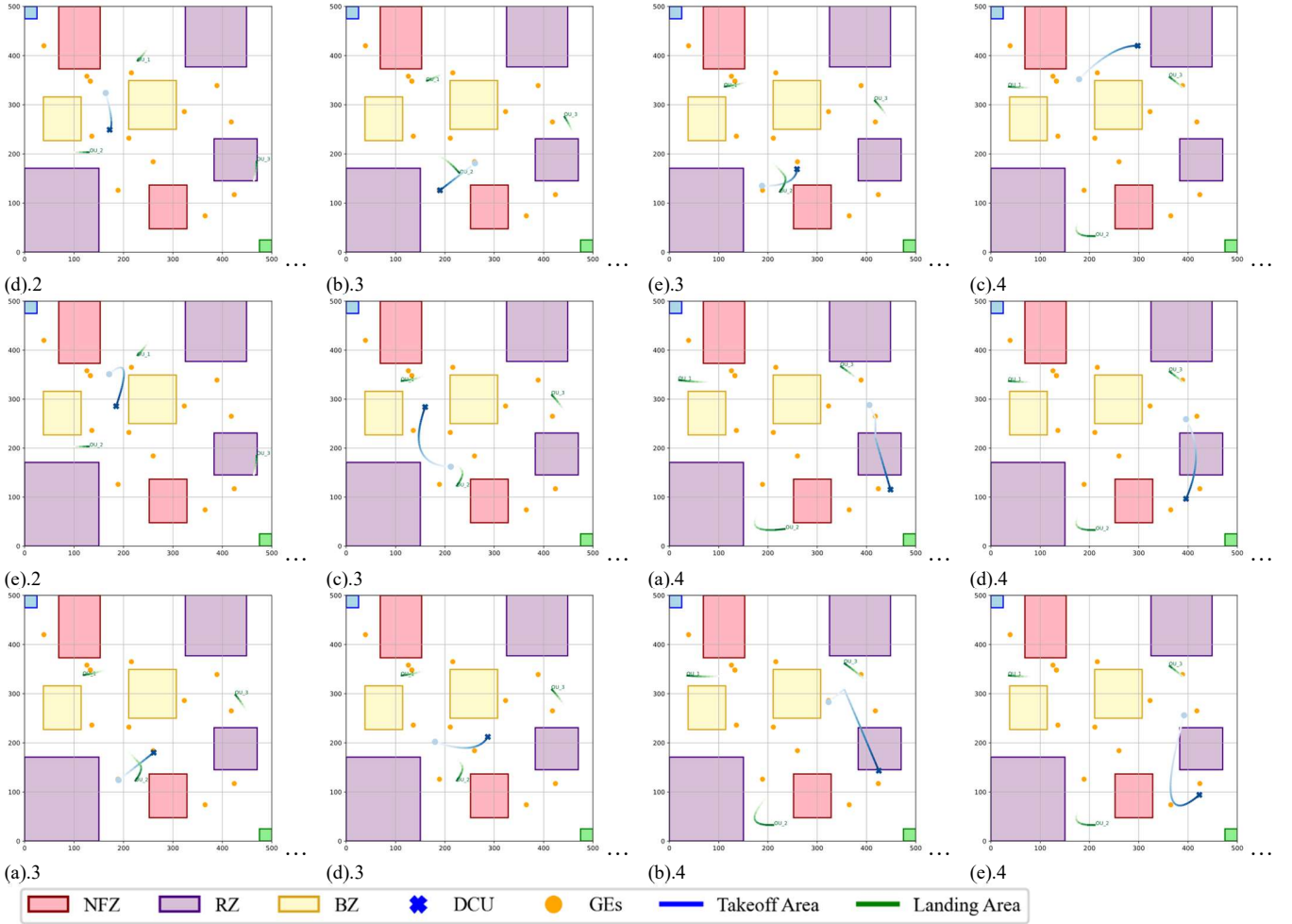


Fig.4 Representative snapshots of DCU flight trajectories during data collection under different algorithms. (a).1-4: **Heuristic**; (b).1-4: **LLM**; (c).1-4: **SAC+LLM (0.3)**; (d).1-4: **SAC**; (e).1-4: **Ours**.

C.2 Metrics about Baselines and Our Algorithm

The experimental results in Figs.5 and 6 comprehensively assess six critical performance metrics, *DCR*, *CR*, *SLR*, *RVR*, *ECR*, and *YR*, under varying numbers of GEs and OUs. These metrics are directly aligned with the core demands of urban low-altitude data collection in the emerging low-altitude economy, where obstacle avoidance (**R2**), compliance (**R3**), and economy (**R4**), mentioned in Section IV.A, are essential.

Our proposed algorithm consistently outperforms all baselines across these metrics, especially as N_{GE} increases. In terms of *DCR*, our method maintains a high *DCR* even in complex environments, showcasing its robustness and superior ability to fulfill **R4**. In contrast, while heuristic and LLM-based approaches successfully avoid collisions (satisfying **R2**), they do so at the cost of significantly reduced data acquisition, prematurely terminating missions due to energy constraints or lack of decision-making flexibility, thus failing to meet the economic demands of **R4**. SAC, while capable of collecting data, often sacrifices safety or legal compliance, leading to increased *CR* and *RVR*, which highlights its limitations under the strict airspace reuse rules required by **R3**.

Furthermore, our method achieves perfect *SLR* and minimal

RVR across all scenarios, underscoring its capacity to complete missions reliably while adhering to regulations. SAC+LLM, by contrast, performs poorly across the board. Its inability to converge and inconsistent behavior stemming from randomly delegated decisions to LLM result in high *CR* and *RVR*, undermining both **R2** and **R3**. Meanwhile, our algorithm demonstrates low *ECR* and high yield *YR*, completing missions with minimal resource consumption and within operational constraints, a critical requirement for economic feasibility under **R4**.

In summary, the results validate that our approach, by selectively engaging LLM for obstacle avoidance, empowers DCU to make informed, adaptive decisions in complex environments. This targeted integration enables our method to uniquely balance the three core demands of the low-altitude economy: high obstacle avoidance (**R2**), strict compliance (**R3**), and economic efficiency (**R4**). No other baseline achieves comparable comprehensive performance. Thus, our approach stands out as a robust, real-world-suitable solution for urban low-altitude data collection tasks.

VII. CONCLUSION

> REPLACE THIS LINE WITH YOUR MANUSCRIPT ID NUMBER (DOUBLE-CLICK HERE TO EDIT) <

In this paper, we propose a novel UAV trajectory planning framework tailored for low-altitude data collection in complex urban environments. Unlike prior works that focus on isolated objectives, our approach jointly addresses three key challenges: obstacle avoidance, regulatory compliance, and economically viable data collection. We modeled the planning task as a partially observable Markov decision process and designed a hybrid optimization algorithm combining soft actor-critic

algorithm with the large language models. Extensive experiments demonstrated the effectiveness of our algorithm in improving data collection performance while reducing collisions, regulatory violations, and energy consumption.

Future research could explore multi-UAV collaborative planning and real-time adaptation to changing airspace conditions to further enhance the practical applicability of our algorithm.

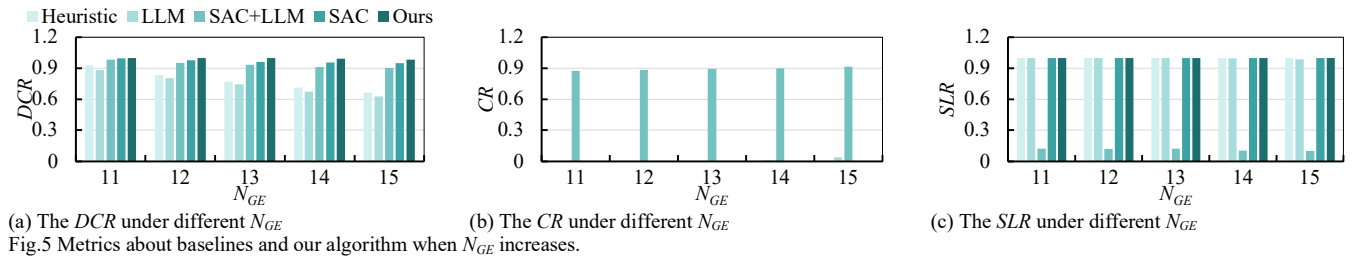


Fig.5 Metrics about baselines and our algorithm when N_{GE} increases.

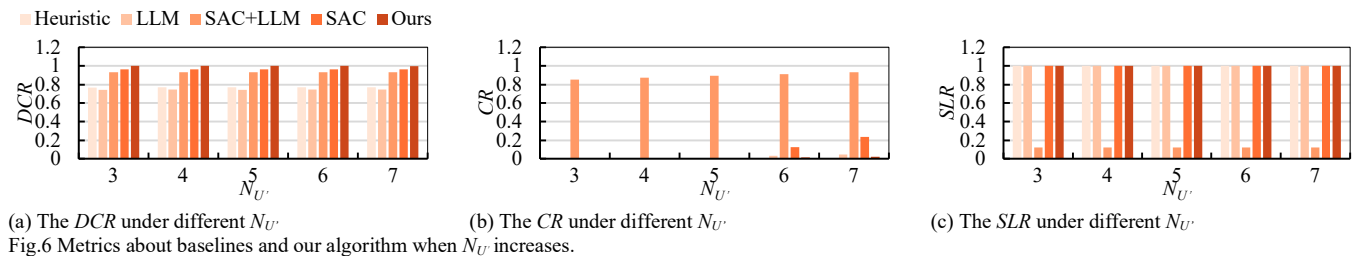


Fig.6 Metrics about baselines and our algorithm when N_U increases.

REFERENCES

- [1]. Y. Jiang, X. Li, G. Zhu, H. Li, J. Deng, K. Han, C. Shen, Q. Shi, and R. Zhang, "Integrated sensing and communication for low altitude economy: Opportunities and challenges," *IEEE Commun. Mag.*, early access, Apr. 2025, doi: 10.1109/MCOM.001.2400685.
- [2]. M. Ahmed, A. A. Soofi, F. Khan, S. Raza, W. U. Khan, L. Su, F. Xu, and Z. Han, "Toward a sustainable low-altitude economy: A survey of energy-efficient RIS-UAV networks," *arXiv preprint, arXiv:2504.02162*, Apr. 2025. [Online]. Available: <https://arxiv.org/abs/2504.02162>.
- [3]. P. Joshi, A. Kalita, and M. Gurusamy, "Reliable and efficient data collection in UAV-based IoT networks," *IEEE Commun. Surveys Tuts.*, early access, Mar. 2025, doi: 10.1109/COMST.2025.3550274.
- [4]. M. Maboudi, M. R. Homaei, S. Song, S. Malihi, M. Saadatseresh, and M. Gerke, "A review on viewpoints and path planning for UAV-based 3-D reconstruction," *IEEE J. Sel. Top. Appl. Earth Obs. Remote Sens.*, vol. 16, pp. 5026–5048, 2023, doi: 10.1109/JSTARS.2023.3276427.
- [5]. N. Zhang, M. Zhang, and K. H. Low, "3D path planning and real-time collision resolution of multicopter drone operations in complex urban low-altitude airspace," *Transp. Res. C Emerg. Technol.*, vol. 129, p. 103123, 2021, doi: 10.1016/j.trc.2021.103123.
- [6]. H. J. Hadi, Y. Cao, K. U. Nisa, Y. Mekdad, A. Aris, L. Babun, A. E. Fergougui, M. Conti, R. Lazerretti, and A. S. Uluagac, "A comprehensive survey on security, privacy issues and emerging defence technologies for UAVs," *Journal of Network and Computer Applications*, vol. 213, p. 103607, 2023, doi: 10.1016/j.jnca.2023.103607.
- [7]. X. Qin, Z. Song, T. Hou, W. Yu, J. Wang, and X. Sun, "Joint optimization of resource allocation, phase shift, and UAV trajectory for energy-efficient RIS-assisted UAV-enabled MEC systems," *IEEE Trans. Green Commun. Netw.*, vol. 7, no. 4, pp. 1778–1792, Dec. 2023, doi: 10.1109/TGCN.2023.3287604.
- [8]. H. Pan, Y. Liu, G. Sun, J. Fan, S. Liang, and C. Yuen, "Joint power and 3D trajectory optimization for UAV-enabled wireless powered communication networks with obstacles," *IEEE Trans. Commun.*, vol. 71, no. 4, pp. 2364–2380, Apr. 2023, doi: 10.1109/TCOMM.2023.3240697.
- [9]. F. Pervez, A. Sultana, C. Yang, and L. Zhao, "Energy and latency efficient joint communication and computation optimization in a multi-UAV-assisted MEC network," *IEEE Trans. Wireless Commun.*, vol. 23, no. 3, pp. 1728–1741, Mar. 2024, doi: 10.1109/TWC.2023.3291692.
- [10]. Y. Zhang, Y. Huang, C. Huang, H. Huang, and A.-T. Nguyen, "Joint optimization of deployment and flight planning of multi-UAVs for long-distance data collection from large-scale IoT devices," *IEEE Internet Things J.*, vol. 11, no. 1, pp. 791–804, Jan. 2024, doi: 10.1109/JIOT.2023.3285942.
- [11]. K. Heo, G. Park, and K. Lee, "Joint optimization of UAV trajectory and communication resources with complete avoidance of no-fly-zones," *IEEE Trans. Intell. Transp. Syst.*, vol. 25, no. 10, pp. 14259–14265, Oct. 2024, doi: 10.1109/TITS.2024.3403887.
- [12]. J. Li, G. Sun, L. Duan, and Q. Wu, "Multi-objective optimization for UAV swarm-assisted IoT with virtual antenna arrays," *IEEE Trans. Mobile Comput.*, vol. 23, no. 5, pp. 4890–4907, May 2024, doi: 10.1109/TMC.2023.3298888.
- [13]. Z. Fu, J. Liu, Y. Mao, L. Q. Qu, L. F. Xie, and X. Wang, "Energy-efficient UAV-assisted federated learning: Trajectory optimization, device scheduling, and resource management," *IEEE Trans. Netw. Serv. Manag.*, vol. 22, no. 2, pp. 974–988, Jun. 2025, DOI: 10.1109/TNSM.2025.3531237.
- [14]. Z. Wang, J. Wen, J. He, L. Yu, and Z. Li, "Energy efficiency optimization of RIS-assisted UAV search-based cognitive communication in complex obstacle avoidance environments," *IEEE Trans. Cogn. Commun. Netw.*, early access, Feb. 2025, doi: 10.1109/TCCN.2025.3544267.
- [15]. S. Silvirianti, B. N. Narottama, and S. Y. Shin, "Layerwise quantum deep reinforcement learning for joint optimization of UAV trajectory and resource allocation," *IEEE Internet Things J.*, vol. 11, no. 1, pp. 430–443, Jan. 2024, doi: 10.1109/JIOT.2023.3285968.
- [16]. R. Liu, M. Xie, A. Liu, and H. Song, "Joint optimization of risk factor and energy consumption in IoT networks with TinyML-enabled Internet of UAVs," *IEEE Internet Things J.*, vol. 11, no. 12, pp. 20983–20994, Dec. 2024, doi: 10.1109/JIOT.2023.3348837.
- [17]. Y. Chen, Y. Yang, Y. Wu, J. Huang, and L. Zhao, "Joint trajectory optimization and resource allocation in UAV-MEC systems: A Lyapunov-assisted DRL approach," *IEEE Trans. Serv. Comput.*, early access, Feb. 2025, doi: 10.1109/TSC.2025.3544124.
- [18]. Z. Ning, Y. Yang, X. Wang, Q. Song, L. Guo, and A. Jamalipour, "Multi-agent deep reinforcement learning based UAV trajectory optimization for differentiated services," *IEEE Trans. Mobile Comput.*, vol. 23, no. 5, pp. 5818–5834, May 2024, doi: 10.1109/TMC.2023.3312276.

> REPLACE THIS LINE WITH YOUR MANUSCRIPT ID NUMBER (DOUBLE-CLICK HERE TO EDIT) <

- [19]. F. Song, M. Deng, H. Xing, Y. Liu, F. Ye, and Z. Xiao, "Energy-efficient trajectory optimization with wireless charging in UAV-assisted MEC based on multi-objective reinforcement learning," *IEEE Trans. Mobile Comput.*, vol. 23, no. 12, pp. 10867–10884, Dec. 2024, doi: 10.1109/TMC.2024.3384405.
- [20]. R. Ding, F. Zhou, Q. Wu, and D. W. K. Ng, "From external interaction to internal inference: An intelligent learning framework for spectrum sharing and UAV trajectory optimization," *IEEE Trans. Wireless Commun.*, vol. 23, no. 9, pp. 12099–12114, Sept. 2024, doi: 10.1109/TWC.2024.3387980.
- [21]. T. Wang, W. Du, C. Jiang, Y. Li, and H. Zhang, "Safety constrained trajectory optimization for completion time minimization for UAV communications," *IEEE Internet Things J.*, vol. 11, no. 21, pp. 34482–34491, Nov. 2024, doi: 10.1109/JIOT.2024.3355906.
- [22]. H. He, W. Yuan, S. Chen, X. Jiang, F. Yang, and J. Yang, "Deep reinforcement learning-based distributed 3D UAV trajectory design," *IEEE Trans. Commun.*, vol. 72, no. 6, pp. 3736–3751, Jun. 2024, doi: 10.1109/TCOMM.2024.3361534.
- [23]. Z. Liu, J. Zhang, Y. Zeng, and B. Ai, "Energy-efficient multi-agent reinforcement learning for UAV trajectory optimization in cell-free massive MIMO networks," *IEEE Trans. Wireless Commun.*, early access, Mar. 2025, doi: 10.1109/TWC.2025.3550266.
- [24]. Z. Ning, H. Ji, X. Wang, E. C. H. Ngai, L. Guo, and J. Liu, "Joint optimization of data acquisition and trajectory planning for UAV-assisted wireless powered Internet of Things," *IEEE Trans. Mobile Comput.*, vol. 24, no. 2, pp. 1016–1030, Feb. 2025, doi: 10.1109/TMC.2024.3470831.
- [25]. Q. Tan, H. Bian, J. Guo, P. Zhou, H. K. Lo, S. Zhong, and X. Zhang, "Virtual flight simulation of delivery drone noise in the urban residential community," *Transp. Res. Part D Transp. Environ.*, vol. 118, p. 103686, Mar. 2023, doi: 10.1016/j.trd.2023.103686.
- [26]. Y. Wang, Z. Wei, H. Wu, and Z. Feng, "Toward Realization of Low-Altitude Economy Networks: Core Architecture, Integrated Technologies, and Future Directions," *arXiv preprint, arXiv:2504.21583*, Apr. 2025. [Online]. Available: <https://arxiv.org/abs/2504.21583>.
- [27]. Z. Wei, M. Zhu, N. Zhang, L. Wang, Y. Zou, Z. Meng, H. Wu, and Z. Feng, "UAV-assisted data collection for Internet of Things: A survey," *IEEE Internet Things J.*, vol. 9, no. 17, pp. 15460–15483, Sept. 2022, doi: 10.1109/JIOT.2022.3182483.
- [28]. D. D. Falconer, F. Adachi, and B. Gudmundson, "Time division multiple access methods for wireless personal communications," *IEEE Commun. Mag.*, vol. 33, no. 1, pp. 50–57, Jan. 1995.
- [29]. Y. Li, "Deep reinforcement learning: An overview," *arXiv preprint, arXiv:1701.07274*, Jan. 2017. [Online]. Available: <https://arxiv.org/abs/1701.07274>.
- [30]. X. Tang, Y. Wang, Q. Huang, Y. Li, and C. Wang, "Highway decision-making and motion planning for autonomous driving via soft actor-critic," *IEEE Trans. Veh. Technol.*, vol. 71, no. 5, pp. 4706–4717, May 2022, doi: 10.1109/TVT.2022.3151651.
- [31]. Q. Zhang, H. Sun, Z. Feng, H. Gao, and W. Li, "Data-Aided Doppler Frequency Shift Estimation and Compensation for UAVs," *IEEE Internet Things J.*, vol. 7, no. 1, pp. 400–415, Jan. 2020, doi: 10.1109/JIOT.2019.2943608.
- [32]. H.-T. Ye, X. Kang, J. Joung, and Y.-C. Liang, "Optimization for Full-Duplex Rotary-Wing UAV-Enabled Wireless-Powered IoT Networks," *IEEE Trans. Wireless Commun.*, vol. 19, no. 7, pp. 5057–5072, Jul. 2020, doi: 10.1109/TWC.2020.2989302.
- [33]. Z. Dai, H. Wang, C. H. Liu, R. Han, J. Tang, and G. Wang, "Mobile crowdsensing for data freshness: A deep reinforcement learning approach," in *Proc. IEEE Conf. Comput. Commun. (INFOCOM)*, May 2021, pp. 1–10.
- [34]. C. Wen, L. Qiu, and X. Liang, "Securing UAV communication with mobile UAV eavesdroppers: Joint trajectory and communication design," in *Proc. IEEE Wireless Commun. Netw. Conf., WCNC*, 2021, pp. 1–6, doi: 10.1109/WCNC49053.2021.9417318.
- [35]. X. Wang, M. C. Gursoy, T. Erpek, and Y. E. Sagduyu, "Collision-aware UAV trajectories for data collection via reinforcement learning," in *Proc. IEEE Glob. Commun. Conf.*, 2021, pp. 1–6, doi: 10.1109/GLOBECOM46510.2021.9686015.
- [36]. S. Rahim, L. Peng, and P.-H. Ho, "TinyFDRL-Enhanced Energy-Efficient Trajectory Design for Integrated Space-Air-Ground Networks," *IEEE Internet Things J.*, pp. 1–1, 2024, doi: 10.1109/JIOT.2024.3361394.
- [37]. Y. Zeng, J. Xu, and R. Zhang, "Energy Minimization for Wireless Communication With Rotary-Wing UAV," *IEEE Trans. Wireless Commun.*, vol. 18, no. 4, pp. 2329–2345, Apr. 2019, doi: 10.1109/TWC.2019.2902559.
- [38]. D. Chen and W. Hua, "Hierarchical VAE Based Semantic Communications for POMDP Tasks," in *Proc. IEEE Int. Conf. Acoust., Speech Signal Process. (ICASSP)*, Apr. 2024, pp. 5540–5544. doi: 10.1109/ICASSP48485.2024.10445833.
- [39]. DeepSeek, "DeepSeek: Large Language Models and Multimodal Intelligence," [Online]. Available: <https://www.deepseek.com/>. [Accessed: May 27, 2025].
- [40]. X. Wang, M. C. Gursoy, T. Erpek, and Y. E. Sagduyu, "Learning-Based UAV Path Planning for Data Collection With Integrated Collision Avoidance," *IEEE Internet Things J.*, vol. 9, no. 17, pp. 16663–16676, Sep. 2022, doi: 10.1109/JIOT.2022.3153585.
- [41]. J. Fan, X. Chang, J. Mišić, V. B. Mišić, T. Yang, and Y. Gong, "Energy-constrained safe path planning for UAV-assisted data collection of mobile IoT devices," *IEEE Internet Things J.*, vol. 11, no. 24, pp. 39971–39983, Dec. 2024, doi: 10.1109/JIOT.2024.3448537.